Cellulose
https://doi.org/10.1007/s10570-019-02605-8

ORIGINAL RESEARCH

Simulation of performance of fibrous filter media composed of cellulose and synthetic fibers

Zhengyuan Pan · Yun Liang · Min Tang · Zhaoxia Sun · Jian Hu · Jing Wang

Received: 14 December 2018 / Accepted: 30 June 2019
© Springer Nature B.V. 2019

Abstract Fibrous filter media with reticular support structure and tortuous pore channels have been widely used in filtration fields. Most of these filter media contain multiple types of fibers such as wood pulp fibers, glass fibers or synthetic fibers with a broad range of diameters to meet the requirements of filtration and strength performance. Some fibers in the filter media, e.g. cellulose fibers, have complex and irregular shapes such as hollow structure. It is necessary to generate a more realistic filter media model based on the actual properties of fibers. In this work, fibrous filter media with complex microstructure were investigated by simulation method. SEM (scanning electron microscope) and fiber analyzer were used to obtain the physical characteristics of fiber such as diameter, wall thickness, length Gaussian distributions, and cross-section shape. Based on these experimental data, a database containing several common fiber models was created. 3-D fibrous models corresponding to the real wet-laid binderless filter media were generated. Average pore size, permeability and collection efficiency simulations were carried out using the modules of the GeoDict code. The simulated results were close to the experimental data. With the work of this study, it was found that smaller diameter PET fibers in the filter media led to a lower average pore size, lower permeability and a better collection performance. When the diameter of PET fibers was < 5.54 μm, the change in fiber diameter has a great impact on the performance. When the diameter of PET fibers was larger than 12.40 μm, it has less effect on the performance.

Z. Pan · Y. Liang · M. Tang (✉) · Z. Sun · J. Hu
State Key Laboratory of Pulp and Paper Engineering, South China University of Technology, Guangzhou 510640, China
e-mail: tangminde@163.com

M. Tang
Particle Technology Laboratory, Department of Mechanical Engineering, University of Minnesota, 111 Church St. S.E, Minneapolis, MN 55455, USA

Z. Pan · J. Wang
Institute of Environmental Engineering, ETH Zurich, 8093 Zurich, Switzerland

Published online: 08 July 2019

Graphic abstract

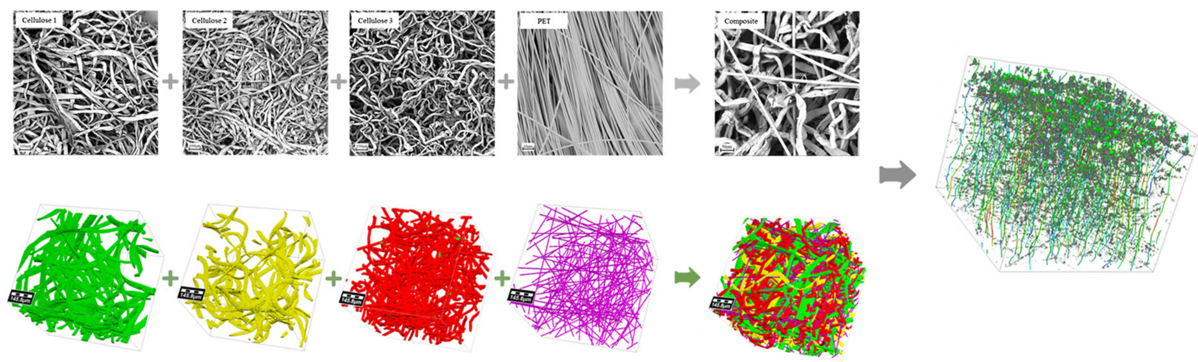

Keywords Cellulose · Fibrous filter media · Fiber model · Simulation · Filtration performance

Introduction

As a well-established effective method to reduce air pollution, filtration using fibrous filter media with reticular support structure and tortuous pore channels that allow airflow to pass through while effectively trapping particles has been widely used in engine industry (Sun et al. 2018), commercial and residential heating and air conditioning (HVAC) systems, clean rooms, personal protection and industrial chemical processing applications. The most common fibers in air filtration include polypropylene (PP), polyester (PET), glass and cellulose. As a low cost and environmentally green material (Jonoobi et al. 2015), cellulose fibers not only provide bulk, permeability and mechanical strength for filter media, but also act as a support structure for the media such as melt-blown and electrospun media which are generally too thin and weak to own structural integrity (Hutten 2016). Cellulose fibers are usually used in combination with other fibers such as synthetic fibers or glass fibers to meet the stringent requirements of filtration and strength performance. Therefore, the knowledge of the performance of fibrous filter media containing multiple types of fibers used in air filtration fields is particularly important.

The theories involved in aerosol filtration with fibrous media are mostly concerned with flow-through porous media and particle filtration. In early research, Davies (1973) simplified the fibrous filter media into single or isolated fibers and offered the single fiber theory to describe the filtration of aerosol particles from an air stream. Kuwabara (1959) and Happel (1959) cell model considered the effects of adjacent fibers and assumed filter media as arrays of randomly distributed parallel circular cylinders. However, these theories and prediction models relied on empirically fitted parameters from assumed conditions. Due to the wide range of operating conditions as well as media type and aerosol characteristics (Zhang et al. 2019), the prediction theories remain hardly achievable. Numerical studies consisting of generating fibrous filter models together with solving general field equations (mass, momentum, energy balance) have been powerful tools to predict the performance of fibrous filter media. The 2-D microstructural model had been introduced for paper-based materials implemented with SEM analysis (Jiang et al. 2018). Chang et al. (2006) carried out series of simulations of particle collection process on 2-D filter models of cylindrical fibers. The 2-D filter model could clearly present the effect of particle capture mechanisms and deposition morphology of particles, but still could not accurately describe the 3-D network structure of actual filter media. Therefore, some scholars developed the virtual 3-D filter media for the filtration simulation. The generation of 3-D filter media model can be classified into two categories. One is to reconstruct the 3-D microstructure based on the parameters such as fiber diameter, fiber length, fiber orientation and porosity of fibrous filter media as input data. The influence of these parameters on the performance of filter media had been investigated (Fotovati et al. 2010a, b; Wang et al. 2007; Hosseini and Tafreshi 2010). However, almost all of these studies assumed the fibers in the virtual 3-D structure as straight cylinders. Moreover, the microstructures of filter media in these studies were simple, and the fibers were usually monodispersed or bimodally dispersed (Fotovati et al. 2010a, b). The other way to reconstruct a 3-D filter media model is by converting the 3-D image data of real filter media from X-ray microtomography (Gervais et al. 2015, 2017), FIB/SEM-scan (Aslannejad et al. 2017) or digital volumetric imaging (DVI) (Jaganathan et al. 2008), etc. into 3-D media models. The advantage of these methods is that realistic filter geometries can be simulated, but there are still some problems. First, there is a conflict between the spatial resolution and the field size, since high resolution means small spatial domain size. Second, the uniqueness of each filter makes it difficult to parameterize or characterize the reconstruction of filter media, and each individual reconstruction is difficult to obtain (Yang et al. 2018). Third, if a filter medium is composed of several kinds of fibers with similar X-ray absorption contrast, it is difficult to distinguish each fiber and parameterize the fiber by image processing. For example, it is difficult to determine the parameters of each fiber like density, Hamaker constant, etc.

In this work, we developed a method to reconstruct the 3-D fibrous structures of the actual composite filter media containing multiple types of cellulose fibers and polyester fibers. The generation of the virtual 3-D fibrous structures corresponding to above composite filter media was divided into two steps. Firstly, SEM and fiber analyzer were used to obtain the physical characteristics of fibers. Based on these experimental values, a database containing parameters of several common fiber models was created. Then the macroscopic parameters of filter media models such as domain size, basis weight, fiber percentage, voxel length were determined according to the experiment data. The measured results such as average pore size, permeability and filtration efficiency were compared with the simulated results using the modules of Geodict code. Based on this work, we can continue to increase the number of types of fiber raw materials in the database, which can help to develop high performance filter media from plenty of fiber combinations and internal structure designs for different application.

Experiment

Materials and samples preparation

In air filtration, synthetic fibers and cellulose fibers are most commonly used to manufacture filter media. In this study, five binderless fibrous filter media, made of three types of cellulose fibers and five different polyester (PET) fibers, were prepared by the wet-laid process. The filter media was designed according to the commercial filter medias provided by Fibrway company (Guangzhou, China). In each filter medium, the cellulose fibers were the same, while the PET fibers were with diameters of 2.9 µm, 5.5 µm, 8.5 µm, 10.9 µm, 17.4 µm, respectively. The mass ratio of cellulose fiber to PET fiber is 95:5, and the basic weight of each filter medium is 100 g/m^2. The surface morphologies of the fibrous filter media are characterized by scanning electron microscope (G2 Pro Y, Phenom-World, Netherlands). As seen in Fig. 1, while the cellulose fibers were irregular in shape, the PET fiber had regular morphology. These fibers oriented randomly to form a fiber-web structure, which could serve as a channel for the air flow and capture particles with several coupled filtration mechanisms.

Fiber characterization

Unlike synthetic fibers, the cellulose fibers usually have complicated and irregular shapes, and the cross-section shape of wood pulp fiber is approximately elliptical with a hollow structure. Therefore, it is not practical to simply assume cellulose fibers in the filter media as straight cylinders.

In this study, the size distributions of fiber diameter and wall thickness of three wood pulp fibers were determined by measuring 30 fibers in a SEM image via image analysis software Image-Pro. The fiber analyzer (FS 300, Metso, Finland) was used to determine the fiber length, curl and coarseness by analyzing the fiber suspension. Then the fiber density can be derived by Eq. (1).

$$\rho_f = \frac{C}{\pi d_{f1} d_{f2}} \tag{1}$$

where ρ_f is fiber density; C is the fiber coarseness, which is the mass per unit length; d_{f1} is the major diameter of the elliptical cross-section of fiber; d_{f2} is the minor diameter of the elliptical cross section of the

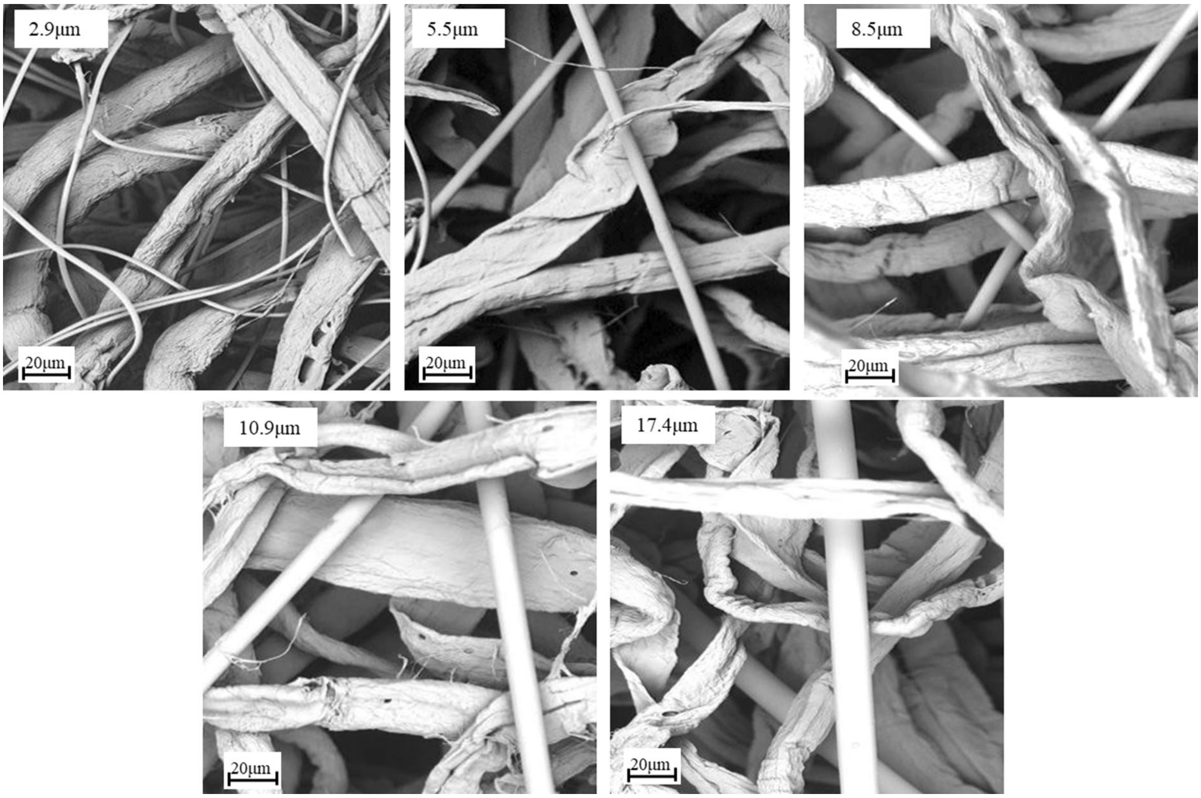

Fig. 1 SEM images of filter media containing PET fibers with different diameters

fiber. Table 1 summarizes the morphological parameters of fibers constituting the filter media. The parameters of cellulose fibers are determined by above methods, and the parameters of PET fibers are provided by the manufacturer.

Filter media characterization

The thickness and basis weight of PET fibrous filter media is summarized in Table 2. The thickness is defined as the vertical surface-to-surface distance of filter media, which has a certain influence on the air permeability and filtration performance. In this study, the average thickness of fibrous filter media was measured using a handheld thickness gauge (YG 142,

Table 2 Fibrous filter media composed of PET fibers with different diameters

	#1	#2	#3	#4	#5
PET diameter (μm)	17.4	10.9	8.5	5.5	2.9
Thickness (μm)	600	633	692	751	768
Basis weight (g/m^2)	100	100	100	100	100

Table 1 Morphological parameters of different fibers

Parameter	Cellulose 1	Cellulose 2	Cellulose 3	PET
Major diameter (μm)	32.87 ± 5.9	26.8 ± 4.3	15 ± 2.5	–
Minor diameter (μm)	13.36 ± 2.9	9.57 ± 2.9	14 ± 5.1	–
Wall thickness (μm)	4.80 ± 1	5.00 ± 1	9.00 ± 1	–
Length (mm)	880	2000	880	5000
Density (g/m^3)	1.4	1.3	1.01	1.38
Curl (%)	15.4%	9.7%	19.1%	0

Ningbo Textile instrument Factory, China) in accordance with the method of TAPPI T411-76.

Pore size measurement

A capillary flow porometer (GFP-1100-A, PMI, USA) based on liquid extrusion technique was used to determine the mean pore sizes, and porewick™ was used as the test liquid. Pore size measurement assumes cylindrical capillaries through the medium, and the mean flow pore size is the pore diameter at which the flow through a wetted medium is 50% of the flow through the dry medium at the same pressure drop.

Filtration performance determination

Air permeability of fibrous filter media is the measured airflow through a specified area of filter media at a specified pressure drop. In this study, the permeability of filter media was determined with an automatic air permeability tester (FX 3300, TEXTtest, Switzerland), and the specified pressure drop was 200 Pa. The airflow of the instrument measured is based on Eq. (2) (Whitaker 1986).

$$v_0 = -\frac{k}{\mu}\frac{\Delta p}{L} \tag{2}$$

where v_0 is the airflow velocity; Δp is the pressure drop; k is permeability constant; μ is the viscosity of air; L is the thickness of filter media.

An automated filter media penetration tester (8130, TSI, USA) was employed to evaluate the filtration efficiency of fibrous filter media. The test flow velocity was 5.34 cm/s, and the test particles were sodium chloride aerosols. As seen in Fig. 2, solid sodium chloride particles were generated by the aerosol generator, supplied with compressed, dry and filtered air and with a 2% solution of NaCl. The generated particles were dried in a dryer chamber and then flew through a neutralizer to reach Boltzmann Charge Equilibrium. The filter media were fixed in a circular sample fixture with test area of 100 cm^2. The air-particle flow entering into the tester was regulated by the mass flowmeter. Two photometers were used to measure the amount of NaCl particles upstream and downstream by light scattering. Counting filtration efficiency was expressed by the percentage of contaminant removal as in Eq. (3).

$$E = 1 - \frac{N_{down}}{N_{up}} \tag{3}$$

where N_{down} and N_{up} were the downstream and upstream concentration of particles, respectively.

Numerical simulations

The simulation tool GeoDict (Math2Market, Germany) was used in this part to simulate the filtration performance of the fibrous filter media. GeoDict was a voxel-based highly integrated software package for material modeling, visualization and property analysis.

Creation of virtual fibrous filter media

PaperGeo module of GeoDict dedicated to generating paper models was used to create the virtual fibrous filter media. As shown in Fig. 3, the creation process was divided into two steps. The fiber models which can represent the real fibers were created, and then the macroscopic parameters of filter media models such as domain size, basis weight, fiber percentage by weight and voxel length were determined. In this study, it was assumed that the fibers in the filter media models were isotropically distributed on the X–Y plane and uniformly laid down in the z-direction. The PET fibers of filter media were assumed to be straight. The voxel numbers in the Z direction were configured according to the thickness of real filter media, basis weight of filter media models and the fiber percentage by weight. The cross-section image of real fibrous filter media and virtual structure was showed in Fig. 4. The green, yellow, red, purple objects in the virtual structure were Cellulose 1, Cellulose 2, Cellulose 3 and PET fiber, respectively. It can be observed from the real filter media and virtual structure that Cellulose 1 and Cellulose 2 with aspect ratio of 3 had similar elliptical cross sections and hollow structures, while Cellulose 3 had an approximate circular cross-section. The cross section of the PET fiber was circular.

As seen in the SEM images, the fibers in the real filter media manufactured by wet-laid process showed almost no overlap, i.e. have non-intersecting fibers. However, in the generation process of filter media models, the algorithm under "allow objects overlap" was fast, and the algorithm under "prohibit object

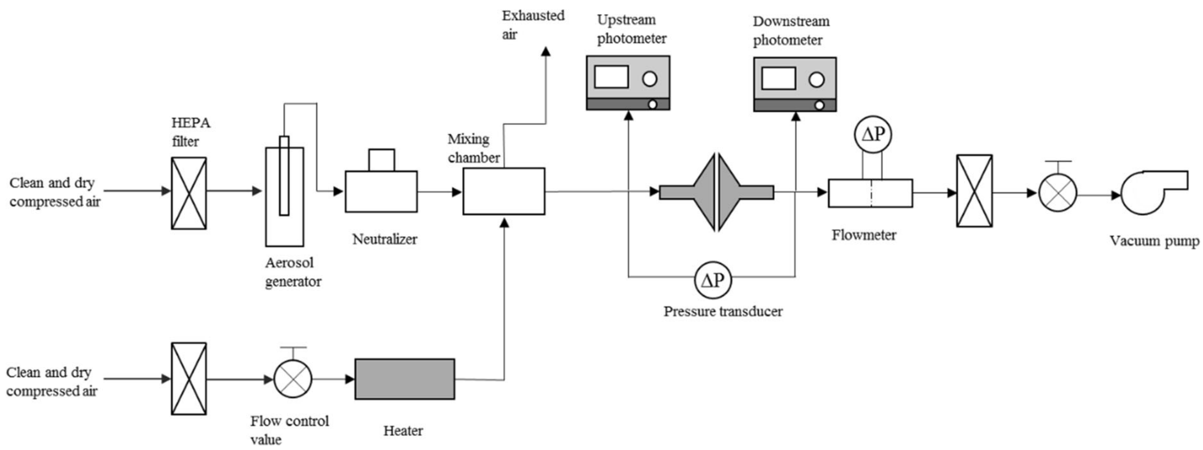

Fig. 2 Schematic of the filtration efficiency tester in the experiment

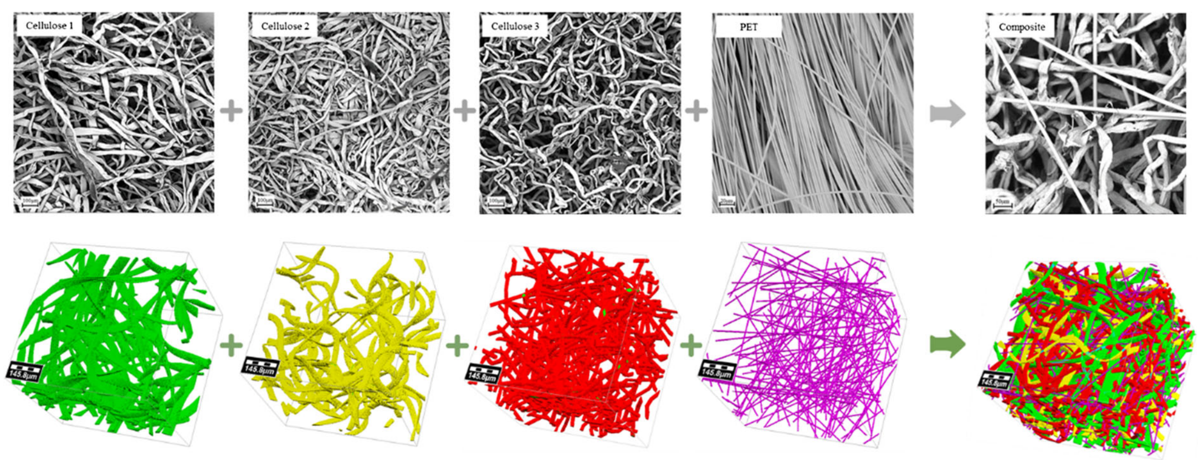

Fig. 3 The creation process of virtual fibrous filter media models

overlap" or "remove fiber overlap" was time-consuming (Wiegmann et al. 2017). Therefore, the effect of volume fraction of fiber overlap on the characteristics such as permeability and average pore size was studied. The generated models with overlap volume fraction of 0.62 and 0.005 were shown in Fig. 5, respectively. When the fraction was 0.005, the overlap between fibers in the filter media models was nearly removed. It is found that the permeability and average pore size of filter media showed a decreasing trend with the decline of overlap volume fraction in Fig. 6. Since the virtual structures with different overlap volume fractions were generated with the same random seed, they had same fiber networks. Therefore, when the overlap volume fraction decreased, the fibers were gradually separated, leading to the decrease of porosity which can be seen in the dot line of Fig. 6. When the volume fraction was lower than 0.01, the porosity and the structure of the filter media tended to be stable. In this work, the overlap volume fraction was kept below 0.01 and the overlap between the fibers was removed.

Representative domain size

Numerical simulations require extensive system memory and computation time. Hence, it is important to find the representative domain size which can accurately predict the performance of filter media models such as pore size distribution, pressure drop and filtration efficiency. The representative domain size is the smallest domain size which represents the

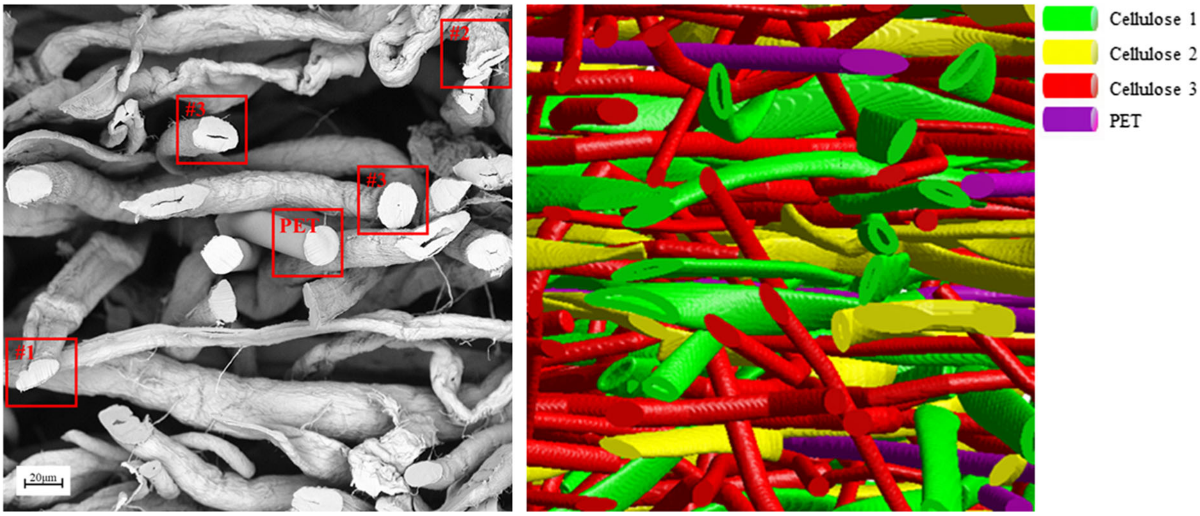

Fig. 4 The cross-section image of real fibrous filter media and virtual filter media model (#1: Cellulose 1, #2: Cellulose 2, #3: Cellulose 3)

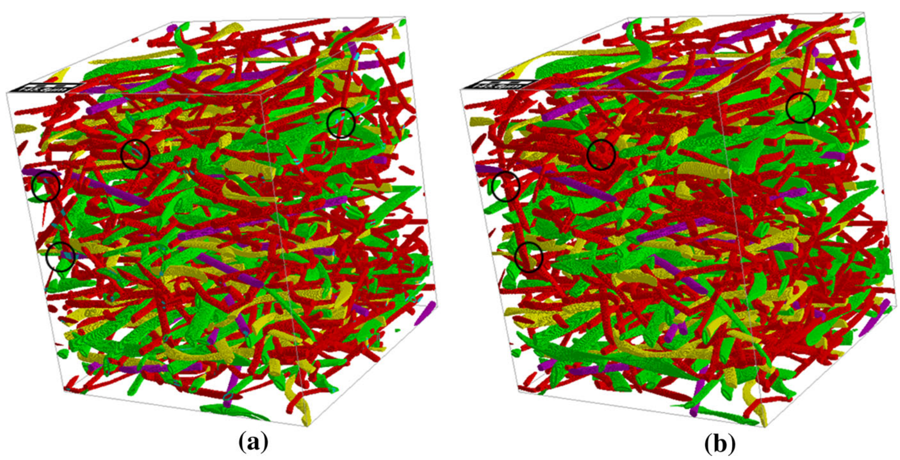

Fig. 5 Generated models with different overlap volume fraction (**a** 0.62, **b** 0.01)

characteristics of domain sizes larger than this size (Lehmann et al. 2016).

Due to the fiber length exceeding even the largest considered domain size, there are some edge effects in the stochastic model (Easwaran et al. 2016). To avoid these edge effects, domain sizes larger than the required sizes were generated and boundary regions of side length smaller than 100 μm were removed. The physical properties such as average pore size, air permeability of generated filter media models with different domain sizes were shown in Fig. 7. Both average pore size and air permeability became stable when domain size reached to 700 μm × 700 μm × 600 μm.

Pore size simulation

As mentioned above, the capillary flow porometer used to determine the mean pore sizes was based on the principle of the liquid extrusion. Only throat of the pore was measured by this method. In the simulation of pore size distribution, a voxel should be completely included in the pore space.

Flow simulation

Flow simulation options were controlled with the FlowDict module of GeoDict. To calculate the airflow through the filter media model, it was assumed that the airflow was purely viscous, incompressible and

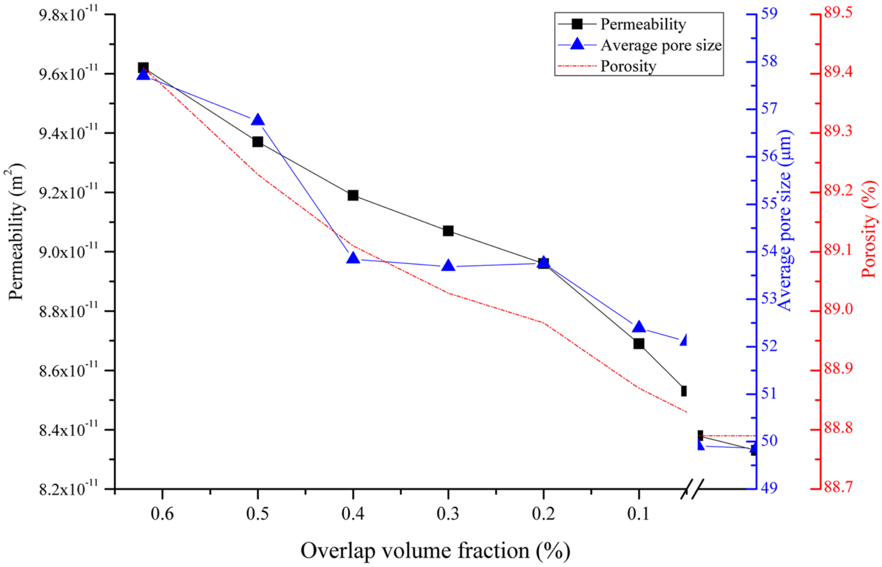

Fig. 6 Permeability and average pore size of filter media models with different overlap volume fraction

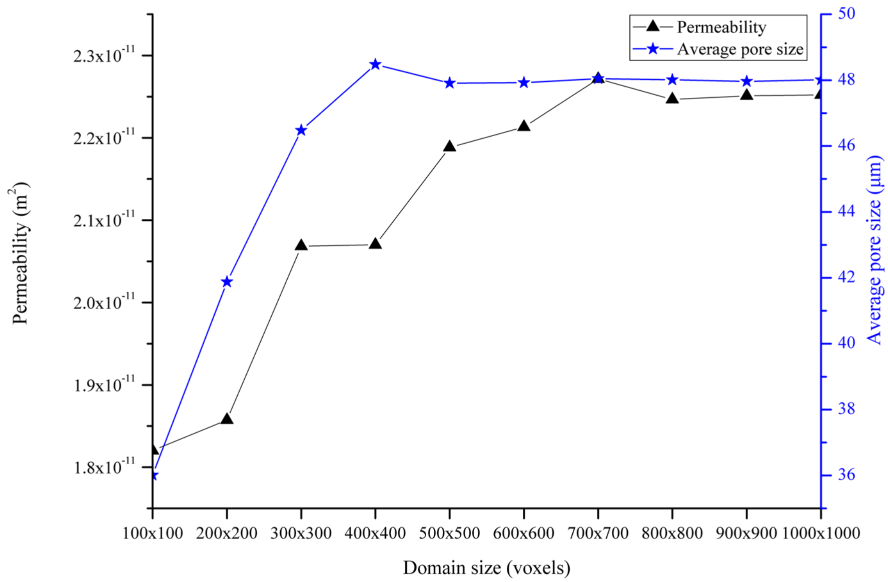

Fig. 7 The permeability and average pore size of generated filter media models with different domain sizes

stationary fluid. For filter media models in this paper, the calculated dimensionless Reynolds number was much < 1, which meant that the airflow through the microstructure can be considered as creeping flow. Therefore, conservation of mass (Eq. (4)) and conservation of momentum (Eq. (5)) can be given as Stokes equations in the pressure and velocity formulations as following (Glowinski and Pironneau 1992):

$$\nabla \overrightarrow{u} = 0 \tag{4}$$

$$-\mu \Delta \overrightarrow{u} + \nabla p = \overrightarrow{f} \tag{5}$$

where $\overrightarrow{u}$ is the fluid velocity; p is the pressure; μ is the fluid viscosity; $\overrightarrow{f}$ is a force density.

When the Stokes equations, simplified from Navier–Stokes equations by dropping the inertial term, were used to describe the flow, change of pressure drop or velocity by a factor can linearly change the other by the same factor. The permeability of the material can be computed by using the Darcy' law expressed as Eq. (6) (Whitaker 1986).

$$Q = \frac{-kA}{\mu}\frac{(P_b - P_a)}{L} \quad (6)$$

where Q is fluid flux; k is the intrinsic permeability of the media; A is the cross-sectional area to flow; $(P_b - P_a)$ is total pressure drop; L is the length over where the pressure drop is taking place.

Considering the air thermal conditions and fiber diameters, the Knudsen number is much < 0.0001. The no-slip boundary condition was used as Eq. (7) (Brunner et al. 2006).

$$\vec{u} = 0 \quad (7)$$

To keep the operating parameters in the flow simulation the same as the experiment, the pressure at the gas inlet in the z-direction was set to 0 Pa, and the pressure at the outlet was 200 Pa. The air density and dynamic viscosity were set to 1.204 kg/m^3 and 1.834×10^{-5} kg/(m s).

LIR (Left Identity Right) solver was used to calculate the flow in the computational domain representing the real filter media. The solver used a non-uniform adaptive mesh, and PDEs with local linear systems were solved in very low memory requirements and fast calculation speed (Linden et al. 2015). The periodic boundary conditions in flow direction and tangential direction were used, and the added implicit in-flow region was 10 voxels and implicit out-flow was 10 voxels (Azimian et al. 2018).

The error bound stopping criterion, which can recognize oscillations in the convergence and prevent premature stopping at local minima or maxima, was chosen as the stopping criterion for the flow simulations, and it was set to 0.01. The LIR solver would stop when the relative difference with respect to the prediction was smaller than 0.01. The simulation results were calculated by a workstation with 128 G RAM and four parallel processors, and the calculation time on the computational domain size from $700 \times 700 \times 600$ voxels to $700 \times 700 \times 768$ voxels was about 20 to 50 min. The voxel length was 1 μm.

Filtration efficiency simulation

FilterDict module of GeoDict was used for the filtration efficiency simulation. As it is known, the two most important parts of the filtration efficiency simulation were the movement of the particles in the fluid and the treatment of interactions between the particles and the fibers (collision models) (Rief et al. 2006). In this study, the concentration of the particles is low enough to ignore the interaction among the particles. The particles did not influence the airflow and collide with other particles. The movements of particles mainly resulted from hydrodynamic drag forces from surrounding airflow, Brownian force due to random diffusion, and inertia. Electrostatic effects were not considered. Therefore, the particle motion in the fluid can be described by solving the Lagrangian formulation, and were governed by a force balance acting on each of them, and it can be given as Eq. (8).

$$m\frac{d\vec{v}}{d\vec{t}} = 6\pi\mu\frac{R}{Cc}\left(\vec{u} - \vec{v} + \sqrt{2D}\frac{d\vec{W}(t)}{dt}\right) \quad (8)$$

where m is the particle mass; R is the particle radius; $\vec{u}$ is the fluid velocity; $\vec{v}$ is the particle velocity, D is the diffusivity; dW is 3D Wiener measurement, a mathematical model that describes a continuous-time stochastic process; in the friction coefficient, $Cc = 1 + \frac{\lambda}{R}(1.17 + 0.525e^{-0.78\frac{R}{\lambda}})$ is the Cunningham correction factor (He and Ahmadi 1999); λ is the mean free path of gas molecules.

The interaction between the particles and the fibers was described by the collision model. In the simplest setup, once a particle was in contact with the fiber, it was captured by the fiber. In this study, the Hamaker model, which considered the inelastic collision and adhesion forces between fibers and particles, was used for the simulation of filtration efficiency (Latz and Wiegmann 2003). In the Hamaker model, the velocity of the particles was compared to the adhesive forces. If the speed of the particle was sufficiently small when touching the fiber, the particle was captured by the fiber. The condition on the velocity can be given as Eq. (9).

$$v^2 < \frac{H}{4\pi\rho a_0 R^2} \quad (9)$$

where is ρ the particle density; a_0 is the adhesion distance or equilibrium spacing between the particle and the surface with a typical value of 0.4 nm; R is the particle radius; H is the Hamaker constant (adhesion), which can be given by the Lifshitz theory of van Der Walls forces for the system of spherical particle and the flat impaction surface as Eq. (10) (Israelachvili 2011).

$$H = \frac{3}{4}k_B T\left(\frac{\varepsilon_1 - \varepsilon_3}{\varepsilon_1 + \varepsilon_3}\right)\left(\frac{\varepsilon_2 - \varepsilon_3}{\varepsilon_2 + \varepsilon_3}\right) + \frac{3hv_e}{8\sqrt{2}}\frac{(n_1^2 - n_3^2)(n_2^2 - n_3^2)}{\sqrt{(n_1^2 + n_3^2)(n_2^2 + n_3^2)}\{\sqrt{(n_1^2 + n_3^2)} + \sqrt{(n_2^2 + n_3^2)}\}} \tag{10}$$

where k_B is the Boltzmann constant; T is the absolute temperature; ε is the relative permittivity; η is the refractive index; h is the Plank constant; v_e is main electronic absorption frequency. The values of Hamaker constant calculation were listed in Table 3.

The amount of energy that was not absorbed by the particle-fiber collision was determined by restitution value. The restitution value ranged from 0 to 1. If the restitution value was 1, it meant that no energy was lost and the particle was rebound with the same speed it had before the collision. In this work, the restitution value for particle-fiber interaction was set to 0.1 (Maddineni et al. 2018). The parameters used in the filtration efficiency simulation were summarized in Table 4.

Numerical simulation validation and discussion

Experimental results

The physical characteristics of fibrous filter media manufactured by wet-laid method had been summarized in Table 2. As shown in Fig. 8, the thickness, mean pore size and permeability of filter media showed a decreasing trend with smaller PET fiber diameter.

In the fibrous filter media, the decrease in fiber diameter reduced the space occupied by a single fiber, and the contribution of the fiber to the thickness was reduced, while the increase in the number of fibers caused more fibers to accumulate in z-direction of filter media, both of which affected the thickness of the filter paper. Therefore, when the PET fibers distributed in the structures were increased from 11 to 17 μm, the

Table 3 Parameters for the calculation of Hamaker constant

Parameter	Values
Boltzmann constant, k_B	1.38×10^{-23}
Temperature, T (K)	300
Relative permittivity, ε	Particle (5.90), Cellulose (3.78), PET (2.29), Air (1.00)
Refractive index, η	Particle (1.54), Cellulose (1.54), PET (1.43), Air (1.00)
Plank constant, h (J s)	6.63×10^{-34}
Main electronic absorption frequency, v_e (s^{-1})	3.0×10^{15}

Table 4 Parameters used in the filtration efficiency simulation

Parameter	Values
Air density, ρ_p (kg/m^3)	1.204
Air dynamic viscosity, μ (kg/ms)	1.834×10^{-5}
Particle density, ρ_p (kg/m^3)	2165
Particle diameter, D_p (μm)	0.26
Hamaker constant, $H/(\times 10^{-20})$	Cellulose (8.14), PET (6.67)
Restitution, $I/([0,1])$	Cellulose (0.1), PET (0.1)
Face velocity, u_0 (cm/s)	5.34

Fig. 8 Experimental results of average pore size, permeability and efficiency

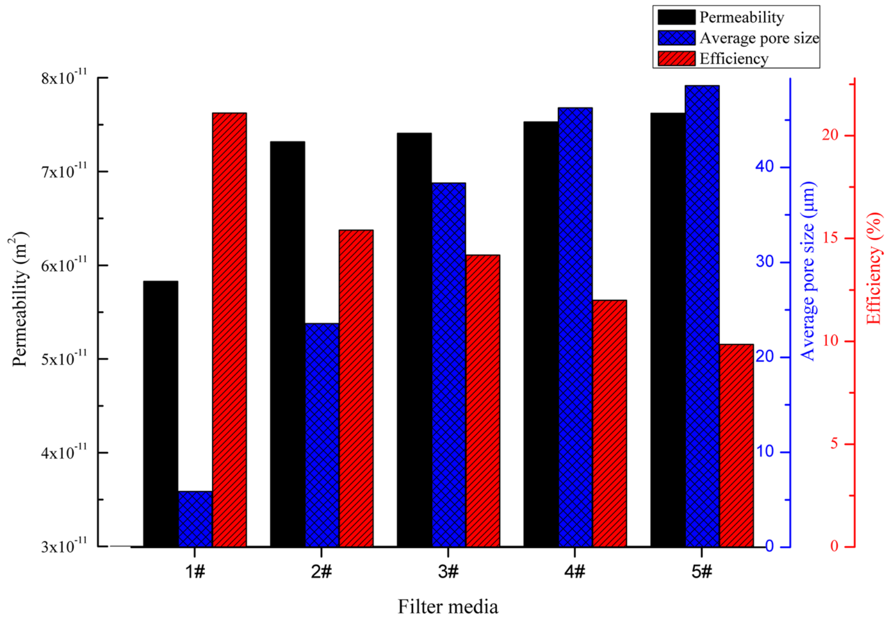

thickness of the filter media increased slightly due to the decrease in the number of fibers. When the PET fiber diameter was sufficiently small, the fibers played a filling role in the filter media and were distributed in the gaps of the cellulose fibers. Therefore, the thickness of #5 filter media decreased slightly compared to #4 filter media.

In air filtration, when basic weight was determined, the fiber diameter was the most important factor affecting the pore structure of filter media (Peart and Ludwig 2000). The number of fibers and number of pores in filter media can be calculated by Eqs. (11) and (12), respectively.

$$N_f = \frac{4M_S}{\pi\rho_f D_f L_f} \tag{11}$$

$$N_p = \frac{16M_S^2 L_f}{\pi^3 \rho_f D_f^4} \tag{12}$$

where the N_f is the number of fibers per unit area of media; D_f is the fiber diameter; M_s is the basic weight of the media; L_f is the fiber length; ρ_f is the density of the fiber; N_p is the number of pores per unit area of media. In this study, the amount of the PET fiber and the number of pores per unit area increased due to the decrease of fiber diameter. Therefore, the mean pore size of filter media declined as the decreasing of the PET fiber diameter. When the airflow passed through the filter media, the amount of energy absorbed by the collision between the air molecules and the fibers increase. Therefore, the air permeability of the filter media decreased.

The filtration efficiency measured by using an automated filter media penetration tester was shown in Fig. 8. As the diameter of PET fibers in the filter media decreased, the filtration efficiency of the filter media increased. This was because that the amount of PET fiber and the number of pores per unit area increased due to the decrease of fiber diameter. When the particles passed through the fiber web structure, the particles were closer to the fiber and the probability of collision between the particles and the fiber was increased. Thus, the filtration efficiency was improved. Meanwhile, the PET fiber with small diameter had large specific surface area, and the probability of particles trapped by random Brownian diffusion increased.

Comparison of numerical calculation and experiments

As mentioned in the above section, the virtual structures corresponding to the real filter media were created, and then the mean pore size, permeability and filtration efficiency of filter media were predicted by numerical simulations. The quantities calculated in this work were all in the through-thickness (TT)

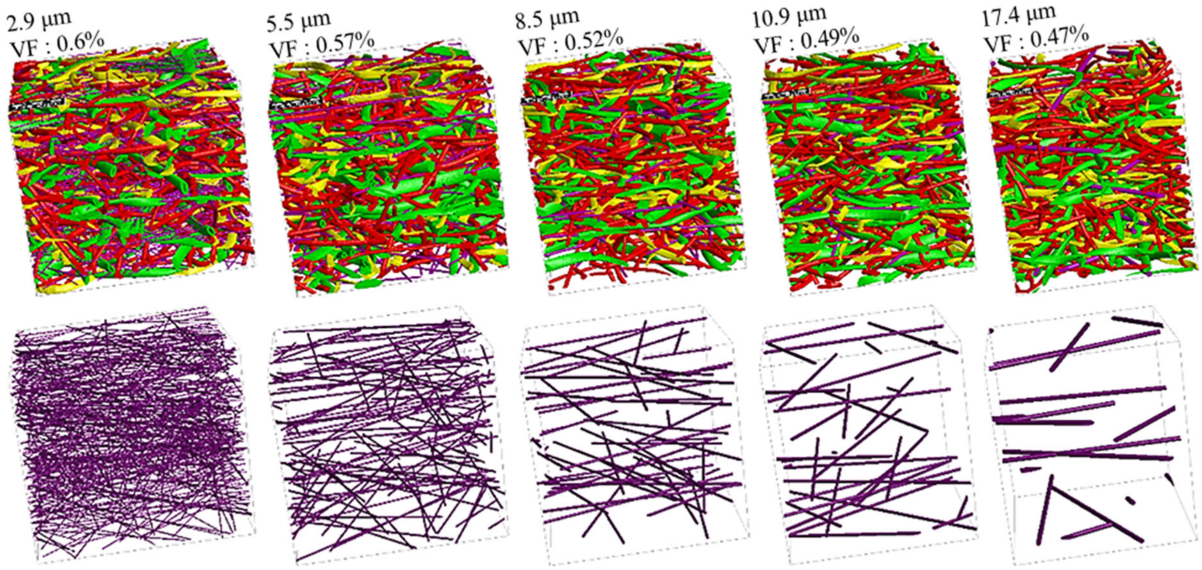

Fig. 9 The 3-D virtual models generated according to the real samples and the web structures formed by PET fibers in the corresponding models

directions. In this section, the simulated values were compared with the experimental results. The 3-D virtual filter media models generated according to the real samples and the web structures formed by PET fibers in the corresponding models were shown in Fig. 9. It can be found that the diameter of PET fibers (violet fiber in Fig. 9) in the filter media models was increasing. As mentioned above, the mass fraction of PET fibers for each filter media was 5%. Due to the increasing thickness of media, the VF (volume fraction) of the PET fibers for each model was 0.6%, 0.57%, 0.52%, 0.49%, 0.47%, respectively.

Pore size

The pores formed by fibers distributed in the filter media were shown in Fig. 10a. The pore structure was represented by the blue block. The pore size of numerical models was the diameter of the bottleneck of through hole in the filter media. Figure 10b compared simulated and experimental results of filter media containing PET fibers with different diameters. The numerical calculation results agreed well with the experimental results. As mentioned in the previous section, the number of PET fibers distributed in the gaps of the cellulose fibers decreased due to the increased diameter, which led to the increase of average pore size. Particularly, when the diameter of PET fibers was 17.4 μm, the number of PET fibers was about 20, which meant that a further increase of the diameter of PET fiber would result in smaller fiber number in the structure. In other words, PET fiber would hardly have effect on the average pore size of the filter media.

Permeability

The permeabilities of virtual filter media composed of three types of cellulose fibers and PET fibers had been calculated by using the FlowDict module of GeoDict. Figure 11a displayed the results of flow simulation for visualization. According to the operating conditions in the experiment, the prediction of mean flow velocity for a given pressure drop was performed. As shown in Fig. 11b, the permeabilities from numerical model are compared with the experimental results. It can be seen that the numerical calculation results agreed well with the experimental results. When the diameter of PET fiber in the filter media decreased, the number of PET fiber increased significantly as shown in Fig. 9, leading to mean decrease of pore size. When the airflow passed through the filter media, the energy absorbed by the collision between air molecules and fibers increased. As a result, the air permeability of the filter media decreased.

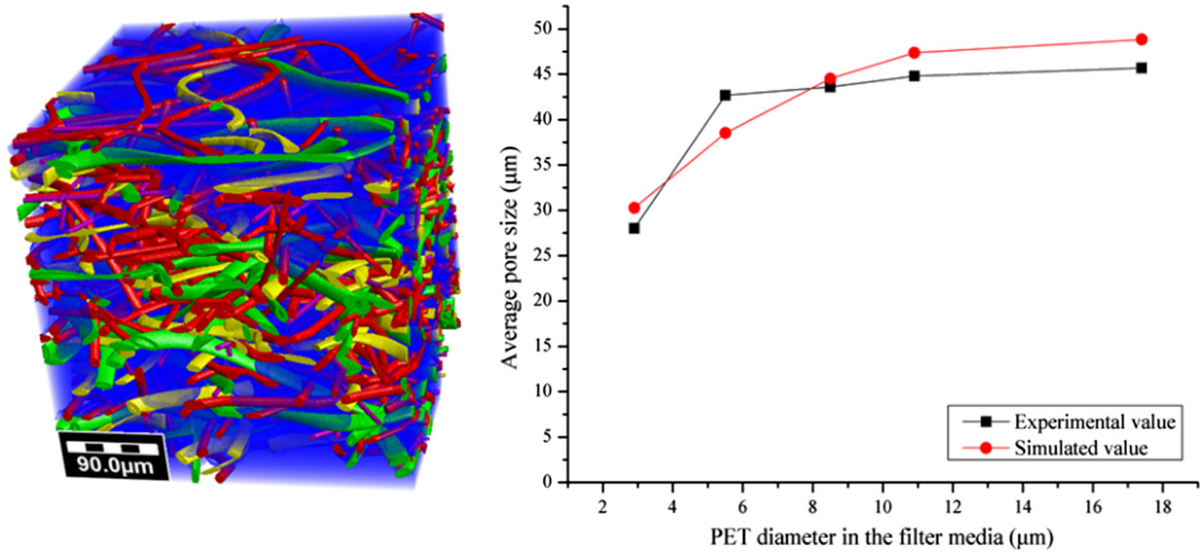

(a) (b)

Fig. 10 Average pore size of the filter media. **a** Pores with 44 µm diameter distributed in the virtual structure corresponding to 3# filter media (blue block). **b** Comparison between experimental and simulated average pore size for filter media containing PET fibers with different diameters. (Color figure online)

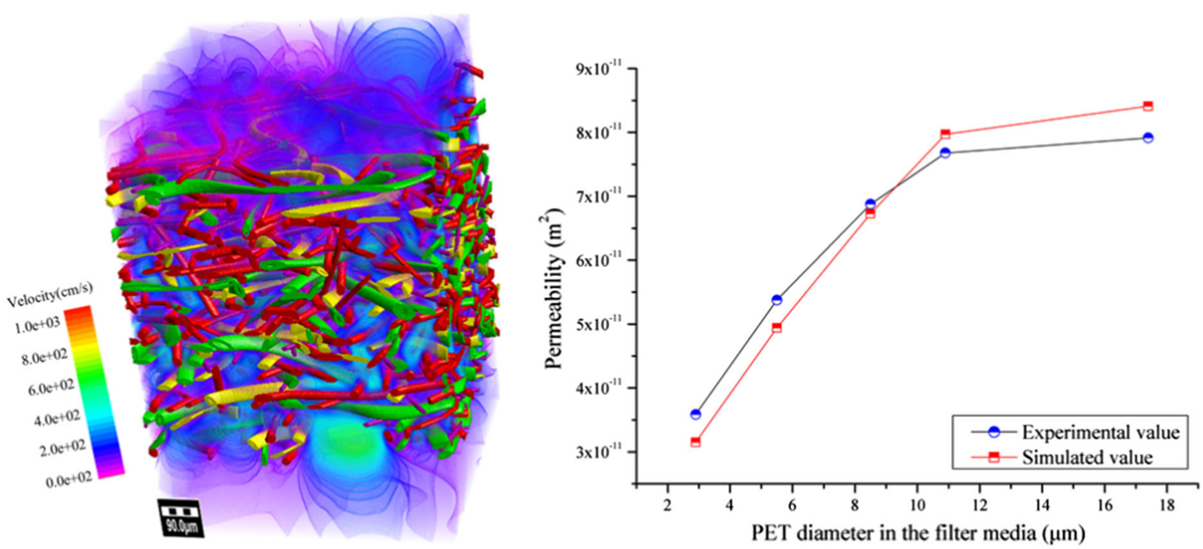

(a) (b)

Fig. 11 Permeability of the filter media. **a** Velocity field of the virtual structure corresponding to #3 filter media. **b** Comparison between experimental and simulated permeability for filter media containing PET fibers with different diameters

Filtration efficiency

The thickness was critical to predict the filtration efficiency of fibrous filter media. In this study, parameters of each virtual filter media were determined by the results of experimental measurements. The trajectory and final position of the particles deposited on fiber were shown in Fig. 12a. As can be seen, the particles were captured by the fibers in the uppermost layer of the filter media, or bypassed these fibers. Figure 12b compared the filtration efficiency results from the numerical simulation and experiment.

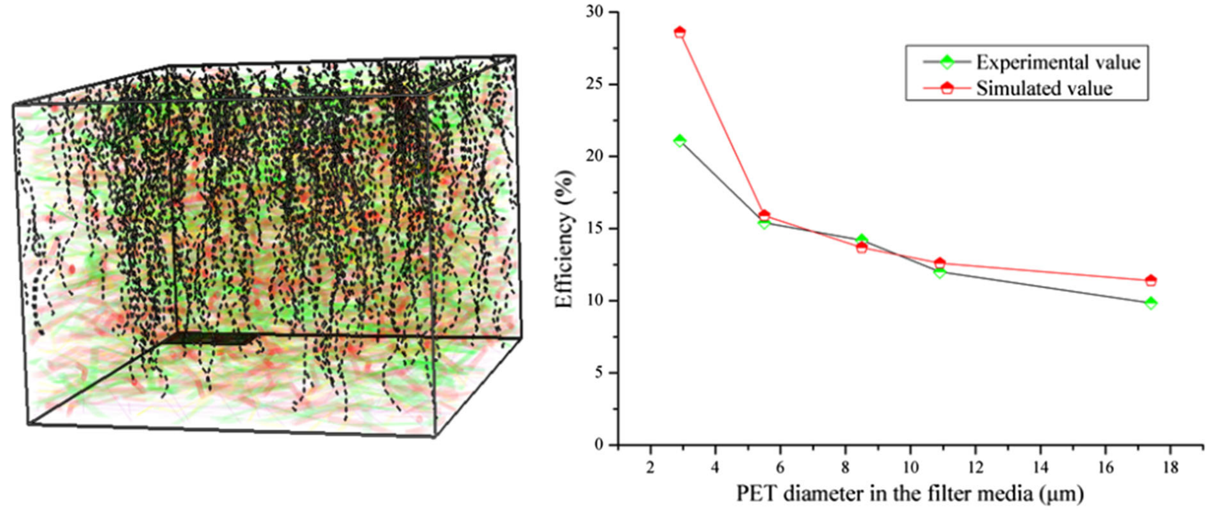

(a) (b)

Fig. 12 Filtration efficiency of the filter media. **a** Trajectory and final position of the particles deposited in the virtual structure corresponding to #3 filter media (black dot lines). **b** Comparison between experimental and simulated filtration efficiency for filter media containing PET fibers with different diameters. (air velocity: 5.34 cm/s, particle size: 0.26 μm)

It can be seen that a good agreement was obtained between experimental and simulated efficiency values when the diameter of PET fibers was larger than 5.54 μm. When the diameter of PET fiber in the filter media was sufficiently small, the simulated value was significantly larger than experimental result. Beside the discrepancy between virtual structure and actual filter media, this behavior could be the results of omitting particle re-entrainment effect (Cleaver and Yates 1976) and fiber dynamics consideration (Xie et al. 2016).

The network structures formed by PET fiber in different filter media were shown in Fig. 9. When the diameter of PET decreased, the amount of fibers increased. These PET fibers distributed in the gaps of the cellulose fibers divided the pore structures of filter media, leading to smaller distance between particles and fiber. Therefore, the filtration efficiency showed an increasing trend with the decrease of diameter of PET fiber in the fibrous filter media.

Conclusions

The reconstruction of the virtual structure of actual composite filter media containing multiple types of cellulose fibers and polyester fibers were studied. The permeability, average pore size and aerosol filtration efficiency were predicted via the airflow and particle transport simulations. Several methods for generation of media models were reviewed. The creation process of virtual structures in this work was divided into two steps. Firstly, the fiber models which can represent the actual fibers were created based on the parameters measured by SEM and fiber analyzer. Secondly, the macroscopic parameters such as domain size, voxel length, fiber percentage by weight were determined with the experimental measurement. We found good agreement between the experimental and simulated results.

With the work of this paper, we explored the feasibility of building a fiber model database. We will continue to increase the number of fiber types in the database, and optimize the filtration performance such as service life time from plenty of fiber combinations and internal structure designs.

Acknowledgments This study was supported by the National Key R&D Program of China (2017YFB0308000). The authors gratefully acknowledge these supports.

References

Aslannejad H, Hassanizadeh SM, Raoof A et al (2017) Characterizing the hydraulic properties of a porous coating of paper using FIB-SEM tomography and 3d pore-scale modeling. Chem Eng Sci 160:275–280

Azimian M, Kühnle C, Wiegmann A (2018) Design and optimization of fibrous filter media using lifetime multipass simulations. Chem Eng Technol 41(5):928–935

Brunner TJ, Wick P, Manser P et al (2006) In vitro cytotoxicity of oxide nanoparticles: comparison to asbestos, silica, and the effect of particle solubility. Environ Sci Technol 40(14):4374–4381

Chang YI, Rong-Shin L, Wei-You C (2006) The deposition morphology of Brownian particles onto a spherical collector. Sep Purif Technol 52(1):126–135

Cleaver JW, Yates B (1976) The effect of re-entrainment on particle deposition. Chem Eng Sci 31(2):147–151

Davies CN (1973) Air filtration. Academic Press, London

Easwaran P, Lehmann MJ, Wirjadi O et al (2016) Fiber thickness measurement in scanning electron microscopy images validated using synthetic data. Chem Eng Technol 39(3):395–402

Fotovati S, Tafreshi HV, Ashari A et al (2010a) Analytical expressions for predicting capture efficiency of bimodal fibrous filters. J Aerosol Sci 41(3):295–305

Fotovati S, Tafreshi HV, Pourdeyhimi B (2010b) Influence of fiber orientation distribution on performance of aerosol filtration media. Chem Eng Sci 65(18):5285–5293

Gervais PC, Bourrous S, Dany F et al (2015) Simulations of filter media performances from microtomography-based computational domain. Experimental and analytical comparison. Comput Fluids 116:118–128

Gervais PC, Bemer D, Bourrous S et al (2017) Airflow and particle transport simulations for predicting permeability and aerosol filtration efficiency in fibrous media. Chem Eng Sci 165:154–164

Glowinski R, Pironneau O (1992) Finite element methods for Navier–Stokes equations. Annu Rev Fluid Mech 24(1):167–204

Happel J (1959) Viscous flow relative to arrays of cylinders. AIChE J 5(2):174–177

He C, Ahmadi G (1999) Particle deposition in a nearly developed turbulent duct flow with electrophoresis. J Aerosol Sci 30(6):739–758

Hosseini SA, Tafreshi HV (2010) 3-D simulation of particle filtration in electrospun nanofibrous filters. Powder Technol 201(2):153–160

Hutten IM (2016) Handbook of nonwoven filter media, 2nd edn. Butterworth-Heinemann, Oxford, UK

Israelachvili JN (2011) Intermolecular and surface forces. Academic Press, London

Jaganathan S, Tafreshi HV, Pourdeyhimi B (2008) A realistic approach for modeling permeability of fibrous media: 3-D imaging coupled with CFD simulation. Chem Eng Sci 63(1):244–252

Jiang F-Z, Weng J, Jia M et al (2018) Microstructural model in COMSOL packages with simulation to aging behavior of paper materials. Cellulose 25(3):1539–1553

Jonoobi M, Oladi R, Davoudpour Y et al (2015) Different preparation methods and properties of nanostructured cellulose from various natural resources and residues: a review. Cellulose 22(2):935–969

Kuwabara S (1959) The forces experienced by randomly distributed parallel circular cylinders or spheres in a viscous flow at small Reynolds numbers. J Phys Soc Jpn 14(4):527–532

Latz A, Wiegmann A (2003) Simulation of fluid particle separation in realistic three-dimensional fiber structures. In: Proceedings of Filtech Europa Düsseldorf, pp 353–360

Lehmann MJ, Weber J, Kilian A et al (2016) Microstructure simulation as part of fibrous filter media development processes–From real to virtual media. Chem Eng Technol 39(3):403–408

Linden S, Wiegmann A, Hagen H (2015) The LIR space partitioning system applied to the Stokes equations. Graph Models 82:58–66

Maddineni AK, Das D, Damodaran RM (2018) Air-borne particle capture by fibrous filter media under collision effect: a CFD-based approach. Sep Purif Technol 193:1–10

Peart C, Ludwig E (2000) The effect of synthetic fiber diameter on number of pores, pore size and efficiency, AFSS Adv Filt Sep Technol 14(272)

Rief S, Latz A, Wiegmann A (2006) Computer simulation of air filtration including electric surface charges in three-dimensional fibrous micro structures. Filtration 6(2):169–172

Sun Z-X, Tang M, Song Q, Yu J, Liang Y, Hu J, Wang J (2018) Filtration performance of air filter paper containing kapok fibers against oil aerosols. Cellulose 25(11):6719–6729

Wang Q, Maze B, Tafreshi HV et al (2007) Simulating through-plane permeability of fibrous materials with different fiber lengths. Modell Simul Mater Sci Eng 15(8):855

Whitaker S (1986) Flow in porous media I: a theoretical derivation of Darcy's law. Transp Porous Media 1(1):3–25

Wiegmann A, Cheng L, Rief S, Latz A, Wagner C, Wersterteiger R (2017) GeoDict user guide. In: PaparGeo, pp 5–10. www.geodict.com

Xie J, Dong M, Li S (2016) Dynamic impact model of plastic deformation between micro-particles and flat surfaces without adhesion. Aerosol Sci Technol 50(4):321–330

Yang H, He S, Ouyang H et al (2018) The pressure drop across combined polydisperse spherical particle—cylindrical fiber networks. Chem Eng Sci 192:634–641

Zhang X, Chen X, Wang J (2019) A number-based inventory of size-resolved black carbon particle emissions by global civil aviation. Nat Commun 10(1):534

Publisher's Note Springer Nature remains neutral with regard to jurisdictional claims in published maps and institutional affiliations.